Solid State Communications 364 (2023) 115134

Contents lists available at ScienceDirect

Solid State Communications

journal homepage: www.elsevier.com/locate/ssc

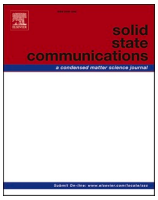

Phase transitions in a polycrystalline compound $Ho_{0.1}Mn_{0.9}S$

O.B. Romanova [a,*], S.S. Aplesnin [a,b], M.N. Sitnikov [b], L.V. Udod [a,b], F.V. Zelenov [b]

[a] Kirensky Institute of Physics, Federal Research Center KSC SB RAS, Akademgorodok, 50, Krasnoyarsk, 660036, Russia
[b] Reshetnev Siberian State University of Science and Technology, Krasnoyarsky Rabochy Av., 31, Krasnoyarsk, 660014, Krasnoyarsk, Russia

ARTICLE INFO

Communicated by: Xu Wen

Keywords:
A. Semiconductors
D. Structural transitions
D. Electronic transitions
D. Mott - Anderson model

ABSTRACT

Sequence of structural transitions in the magnetically ordered region and a displacement-type structural transition at $T = 220$ K accompanied by the variation in the thermal expansion coefficient, ultrasound attenuation coefficient, g factor, and polarization current in the polycrystalline compound $Ho_{0.1}Mn_{0.9}S$ was found. The electronic transitions above room temperature were established on the basis of the measurements of the conductivity, ultrasound attenuation maxima, and IR spectra.

1. Introduction

Manipulating the magnetic, dielectric, and electrical properties of materials by external factors (magnetic and electric fields, temperature, etc.) is one of the important tasks of modern electronics [1,2]. For example, in multiferroics, magnetization is controlled by an electric field and polarization by a magnetic field [3–5].

Manganese chalcogenides with the general formula $Re_XMn_{1-X}S$ (Re = Gd, Ce, Yb, Tm, etc.) are related to strongly correlated systems, in which the magnetotransport effects and phase transitions have been defined [6–12]. Substitution of the rare-earth element holmium for manganese ions in the $Ho_XMn_{1-X}S$ system ($T_N = 134$ K) leads to a sharp decrease in the paramagnetic Curie temperature due to the ferromagnetic s-d interactions [13]. It was found that the magnetic moment at the site decreases at low concentrations. As concentration X increases, the magnetic anisotropy of the $Ho_XMn_{1-X}S$ solid solution grows. The change in the sign of carriers in the range of 210–230 K was established from the Hall-effect measurements [14]. The negative effects of DC - magnetoresistance in the region of the magnetic phase transition and positive AC-magnetoimpedance in the paramagnetic region have been established [15]. The dependence of the magnetoresistance on the concentration and the maximum value at $X = 0.1$ are found. However, the structural and electronic transitions in these compounds have not been studied; therefore, it is necessary to establish mechanism of these transitions and determine their temperatures and the correlation between the transport and structural characteristics. The study of phase transitions of the system $Ho_XMn_{1-X}S$ ($X = 0.1$) will allow to understand magnetotransport effects formation mechanism.

The crystal structure of the compound α -MnS is the NaCl-type face-centered cubic (fcc) lattice [16,17]. It is believed that manganese monosulfide, similar to MnO and NiO, is a second-type antiferromagnetic having the magnetic structure with a unit cell doubled relative to the crystallographic one [18] with a Néel temperature of 150 K [19,20]. The NaCl structure is the cubic closest packing of anions in the planes parallel to (111). The M–S bond length is equal to 2.6 Å. In MnS, each Mn^{2+} ion is bound to the nearest Mn^{2+} ions through the intermediate S^{2-} ions [21]. The octahedra can be distorted at cationic substitution [22,23]. In the compounds with a perovskite structure, an additional displacement of ions is allowed (depending on the symmetry of the position) without changing the space group of the crystal. The displacement of ions from the equilibrium position is determined by interplay magnetic and elastic subsystem.

According to the X-ray diffraction data, the lattice contraction of manganese monosulfide in the temperature range of 125–165 K is accompanied by the rhombohedral distortion below the Néel temperature [20]. The lattice expansion coefficient has anomalies at temperatures of 165, 147, and 125 K caused by the structural changes. The X-ray emission and optical spectra of MnS and the calculated band energies suggested that the upper part of the valence band includes 3 d electrons of the Mn^{2+} ions and 3p electrons of the S^{2-} ions [24]. In manganese monosulfide, the p-type conductivity is implemented due to the impurity states near the valence band.

The aim of this study is to find and elucidate the phase transitions at the substitution of holmium ions for manganese ions in the $Ho_{0.1}Mn_{0.9}S$

* Corresponding author.
E-mail address: rob@iph.krasn.ru (O.B. Romanova).

https://doi.org/10.1016/j.ssc.2023.115134
Received 29 November 2022; Received in revised form 6 March 2023; Accepted 9 March 2023
Available online 10 March 2023

polycrystalline system using the structural, magnetic, transport, optical, and acoustic technique.

2. Material and methods

The $Ho_{0.1}Mn_{0.9}S$ polycrystalline sample were synthesized via melt crystallization of the powder sulfides placed in glassy carbon crucibles in a quartz reactor by pulling the latter through a single-turn inductor of a high-frequency facility. High-purity argon was used as an inert medium. Mixture for crystallization is prepared by mix of the calculated quantities of manganese sulfide and holmium sulfide, preliminary prepared by sulfurizing of corresponding metal oxides by products of NH4SCN thermolysis at temperatures 850–1000 °C. The synthesis procedure was described in detail in Ref. [13].

The microstructure of the sample $Ho_{0.1}Mn_{0.9}S$ was investigated by using a scanning electron microscope (SEM) on a Hitachi SU3500/ Model3500 microscope and a Hitachi S-5500 high-resolution electron microscope and Energy Dispersive X-ray spectroscopy (EDAX) is employed for elemental analysis. The crystal structure of the synthesized $Ho_XMn_{1-X}S$ sample with a substitution concentration of X = 0.1 was investigated by X-ray diffractometry (XRD) at room temperature on a DRON-3 X-ray diffractometer (CuK_α radiation) in the point-by-point data collection mode. The dc measurements of the conductivity were performed on parallelepiped samples in the temperature range of 100–500 K in zero magnetic field. The relative change in the linear sizes of the sample was determined by measuring the electrical resistance of strain gauge located on the sample: $\beta = (1/R_s(T))\ (dR_s(T)/dT) = (1/L_s(T))\ (dL_s(T)/dT)$, where R_s is the electrical resistance of the sample, L_s is the linear size of the sample. The measurements were carried out in a cryostat with an accuracy of temperature stabilization up to 0.02 K using Lake Shore Cryotronics LS Model 224 in the interval 80–500 K. The magnetic properties were investigated on a Quantum Design Physical Property Measurement System (PPMS-9) in a magnetic field of 500 Oe. The IR spectra of the $Ho_XMn_{1-X}S$ (X = 0.1) solid solution were recorded on an FSM 2202 Fourier-IR spectrometer. The measurements were performed on pressed $Ho_{0.1}Mn_{0.9}S$ + KBr tablets 10–20 mm in diameter placed in an optical cryostat in the temperature range of 77–500 K. The ultrasound attenuation in $Ho_{0.1}Mn_{0.9}S$ was measured directly on rectangular samples 8 × 5 × 4 mm in size with two piezoelectric sensors, one used as a generator and the other, as a receiver of the ultrasound waves; the distance between the sensors was l = 4 mm. The ultrasound attenuation coefficient was determined from the ratio between the amplitudes of electric voltage U_{in} at the input and U_{out} at the output of the piezoelectric sensors: $\alpha = \ln(U_{in}/U_{out})/l$. The temperature dependence of the electric polarization was determined on a Keithley 6517 B electrometer from the polarization current in zero electric field along the plane of the sample under preliminarily cooled in an external electric field of 1000 V/cm.

3. Results and discussion

According to the XRD data presented in Fig. 1, the synthesized $Ho_XMn_{1-X}S$ with (X = 0.1) sample have a NaCl-type fcc structure (sp.gr. $Fm\bar{3}m$) with reflections corresponding to cubic α-MnS (JCPDS 03-065-0891). Experimental Kikuchi pattern (insert to Fig. 1) gives crystallographic information about a compound $Ho_{0.1}Mn_{0.9}S$ and confirms date XRD, which point out the formation a FCC phase. Kikuchi patterns are assumed to be formed by incoherent scattering of electrons from the incident beam and subsequent diffraction by the crystal structure [25]. Substitution of holmium ions with a large ionic radius for manganese ions (Mn^{2+} = 0.083 nm, Ho^{3+} = 0.176 nm) leads to an increase in unit cell parameter from a = 0.5219 nm for MnS to 0.5263 nm for $Ho_{0.1}Mn_{0.9}S$.

Microstructural characteristics of the $Ho_{0.1}Mn_{0.9}S$ sample were presented in Fig. 2. The micrographs show uniform microstructure with a

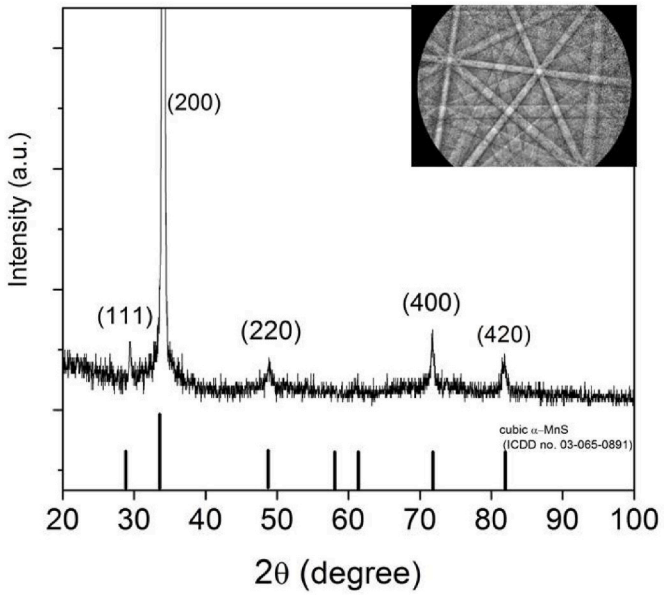

Fig. 1. The X-ray patterns of $Ho_{0.1}Mn_{0.9}S$ samples at T = 300 K and the standard pattern (black sticks) is cubic α-MnS (ICDD no. 03-065-0891). Insert: Experimental Kikuchi pattern of $Ho_{0.1}Mn_{0.9}S$ sample with f. c.c. crystal structure.

smooth surface without formation of separate grains. The chemical composition of the sample surface determined by EDX (Energy Dispersive X - ray Spectroscopy) is given in diagram Fig. 2b. The content and ratio of elements (Ho, Mn and S) in the investigated crystal are almost fully consistent with the calculated data.

The temperature dependence of the conductivity reveals the small maximum at 280 K and anomalies at T_1 = 346 K and T_2 = 446 K (Fig. 3). Jumps of the σ(T) dependence in the paramagnetic temperature region are caused by the substitution of holmium for manganese and not observed in MnS (insert to Fig. 3). The small maximum at 280 K is explained by the depolarization of positively charged structural defects and maximum of the mobility of current carriers. The first jump at T_1 is possibly caused by the formation of charge ordering of electrons and holes associated with the screening of negatively charged impurity centers Ho^{3+}. Decompensating of electric polarization occurs condition when the energy of electrostatic interaction of current carriers and charges on the surface of the cluster is comparable to thermal $W = q^2/2C \sim P^2/2C$, where C - capacitance. In this case, a depolarization current is occurs [26]. The maximum depolarization current at T = 340 K was found in $LuFe_2O_4$ oxides [27].

The second anomaly at T_2 is due to the localization of electrons in potential wells induced by holmium ions. The localization of current carriers is aroused as results of the pinning of lattice polarons by impurity holmium ions [28]. The localization of small hole oxygen-type polarons and their trapping by trivalent dopants (Ga, Sc, In, Lu, Y, Gd, La) was observed in $BaSnO_3$ [29].

The changes in the electronic spectrum and in the structure upon substitution of holmium ions with the larger ionic radius for manganese are accompanied by anomalies in the temperature dependence of the thermal expansion coefficient (Fig. 4). The broad maximum at 120 K corresponds to the structural changes in manganese monosulfide [30]. A sharp increase in the thermal expansion coefficient (β) at T = 220 K is indicative of a possible displacement-type structural transition, i. e., the displacement of atoms of a certain type (in our case, sulfur ions) in the crystal lattice as a result of rotation of the octahedral without changing the space symmetry group of the crystal. Striking examples of such transitions occur in the compounds with a perovskite structure [23,31] and bismuth pyrostannates [32]. In these compounds (pyrostannates), the transition is accompanied by softening of the octahedral vibration

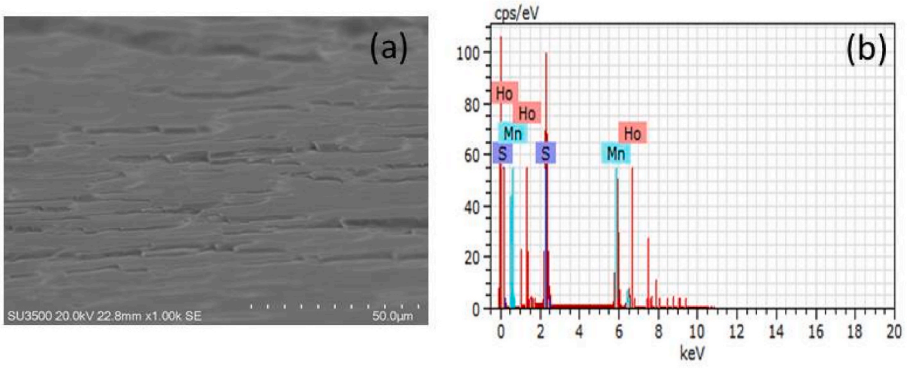

Fig. 2. SEM images of the $Ho_{0.1}Mn_{0.9}S$ sample at 50 μm magnification (a) and EDS spectrum surface of the part of this sample (b).

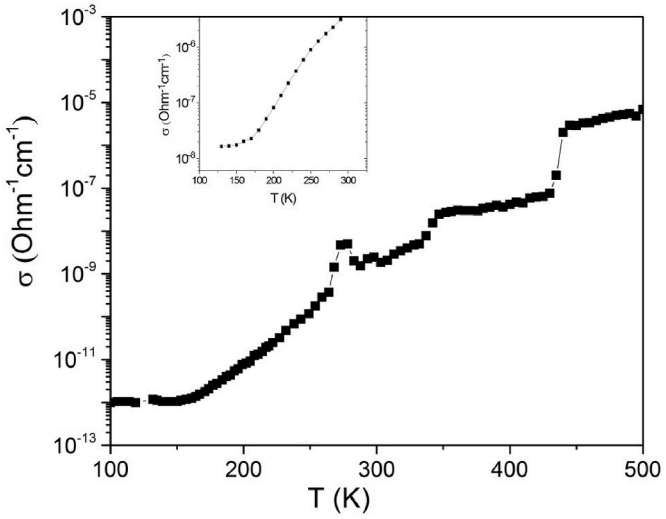

Fig. 3. The temperature dependence conductivity of polycrystalline sample $Ho_{0.1}Mn_{0.9}S$ at H = 0 kOe. Insert: the temperature dependence conductivity of manganese monosulfide at H = 0 kOe.

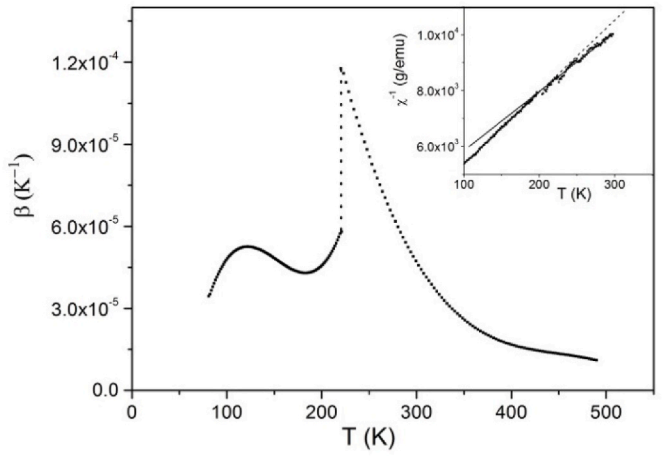

Fig. 4. Thermal expansion coefficient of $Ho_{0.1}Mn_{0.9}S$ versus temperature. Insert: temperature dependence of the magnetic susceptibility measured in a magnetic field 500 Oe for the same sample.

modes and sharp peaks in the temperature dependences of the thermal expansion coefficients and ultrasound attenuation. It was found that, with an increase in temperature, the thermal expansion coefficient nonmonotonically decreases; at 440 K, the derivative of the thermal expansion coefficient has a minimum caused by the localization of electrons.

During the structural transition, the magnetic properties change, and a kink appears in the temperature dependence of the inverse magnetic susceptibility at 220 K (see the inset in Fig. 4). The paramagnetic Curie temperature at T < 210 K is Θ = −108 K and the Curie–Weiss constant is C = 0.039; as the temperature increases, the Θ value attains −152 K at C = 0.045. The growth of the effective moment $\mu_{eff} = g\sqrt{(S(1+S))}$ from 5.5 μ_B to 6 μ_B is due to a change in the g factor. As mentioned above, manganese monosulfide and the $Ho_{0.1}Mn_{0.9}S$ sample synthesized on its basis are antiferromagnets with the second-type ordering, in which the paramagnetic Curie temperature and the Néel temperature have the form $\Theta = 2/3\ S(S+1)\ (Z_1J_1 + Z_2J_2) = A\ (12J_1+6J_2)$; $T_N = A6J_2$, where $J_{1,2}$ is the exchange coupling in the first and second coordination spheres, respectively, and $Z_{1,2}$ is the number of nearest neighbors. A decrease in the absolute value of Θ is aroused as for the change in the exchange couplings.

In the region of the phase transitions, the ultrasound attenuation takes its maximum value. Several maxima caused by the structural and electronic transitions are observed in the temperature dependence of damping coefficient α (Fig. 5). Small jumps at temperatures of 120 and 160 K correspond to the structural transitions observed in the initial matrix of manganese monosulfide MnS [30,33]. The α(T) maximum at T = 225 K is caused by a displacement-type phase transition. The maxima observed at temperatures of 330 and 450 K without field are shifted toward low temperatures in an electric field. The temperatures of α(T)

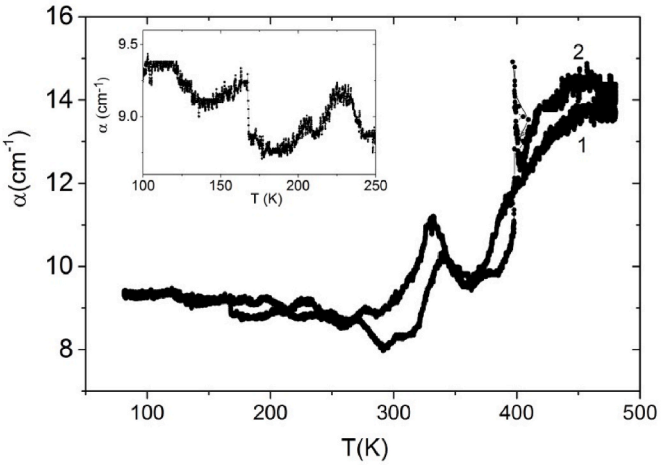

Fig. 5. Ultrasound damping coefficient of $Ho_{0.1}Mn_{0.9}S$ at electric field E = 0 (1) and E = 1000 V/cm (2) versus temperature. Inset: ultrasound damping coefficient in an interval of temperature 100–250 K at E = 0 V/cm for the same sample.

and conductivity maxima are consistent (Fig. 3) and are caused by the charge ordering of electrons and holes at 330 K and electron delocalization at 450 K.

At the displacement-type structural transition, the g factor increases due to the change in the octahedron crystal field and softening of the polar mode, which causes anomalies in the temperature dependence of the polarization. This is proven by the temperature dependence of the polarization current I_p = dP/dT (dT/dt) presented in Fig. 6. The Ip maxima at temperatures of 220 K, and 340 K confirm the occurrence of structural and electronic transitions in the $Ho_{0.1}Mn_{0.9}S$. The softening of the polar mode at 220 K causes a small maximum of the polarization current. The polarization arises from the displacement of sulfur ions similar to manganites [34]. The inset in Fig. 6 shows the piezoelectric field induced by a longitudinal acoustic wave under the action of ultrasound. The sharp maximum at 340 K is caused by the disappearance of the electric polarization and the current of depolarizing charges. The anomaly in the temperature dependence of conductivity detected at 280 K correlates with the maximum polarization current (Fig. 6).

Using IR spectroscopy, we established splitting of the impurity subband. In the high-frequency range of 2900–3100 cm^{-1}, there are two absorption peaks at $\omega_1 = 2917\ cm^{-1}$ and $\omega_2 = 2956\ cm^{-1}$, the intensity of which passes through a maximum upon heating and gradually decreases (Fig. 7). The changes observed in the IR spectra in this frequency range are related to the electronic transitions between the impurity subbands. In the region of 320–360 K, the absorption peaks in the IR spectra vanish because of the disappearance of a gap between the subbands and 4f level shifts to the conduction band (to the edge of mobility).

The temperature of the maximum 220K of the relative change in the intensity of the IR spectra (Fig. 7b) is consistent with the temperature of the maximum of the thermal expansion coefficient and the ultrasound attenuation coefficient. This is due to the change in the spectral intensity of the valence band and impurity subbands during the displacement-type structural transition.

We explain electronic transitions in terms of the Mott - Anderson model [35]. Random replacement of holmium for manganese ions will lead to disorder associated with the arrangement of potential wells, as well as with a random potential. Holmium ion clusters are screened by hole charge carriers, which can be depicted as a set of potential electron and hole wells (Fig. 8a). In the temperature range 330–340 K, the screening of negatively charged centers disappears as a result of thermal fluctuations. Bound electron-hole states are destroyed or dissociated. As a result, the electron and hole density of states are changed in the vicinity of the chemical potential. Holes are delocalized. The radius of the

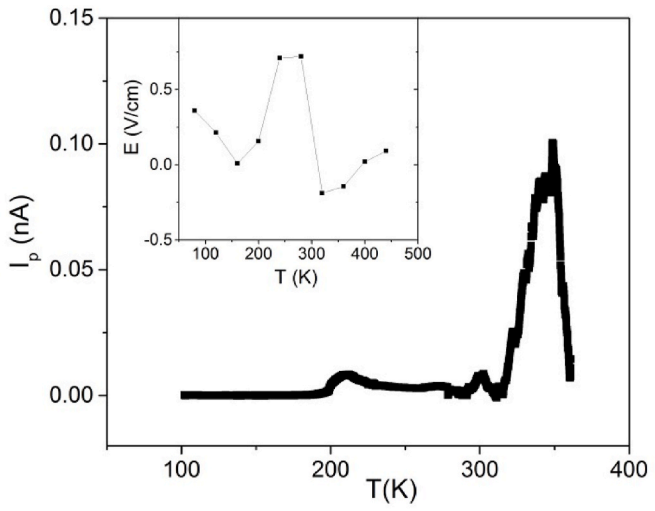

Fig. 6. Polarization current of $Ho_{0.1}Mn_{0.9}S$ versus temperature. Inset: piezoelectric field of sample $Ho_{0.1}Mn_{0.9}S$ versus temperature.

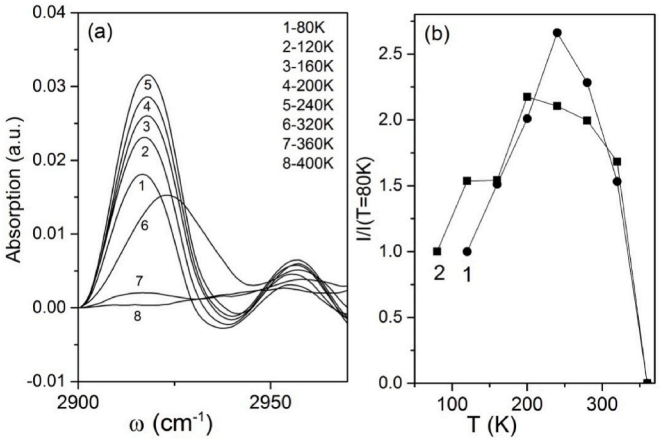

Fig. 7. IR spectra for the $Ho_{0.1}Mn_{0.9}S$ polycrystalline sample (a). The temperature dependence of the IR spectra intensity (b) for the $Ho_{0.1}Mn_{0.9}S$ sample at ω = 2917 cm^{-1} (1) and ω = 2956 cm^{-1} (2).

Coulomb interaction between electrons in potential wells with holmium ions increases, which leads to the splitting of the density of states (Fig. 8b). Upon further heating, the lattice polaron is undraped from the charged holmium potential, where the driving force is the competition between the Coulomb and elastic interactions. At 450 K, the expansion of the lattice increases the elastic energy by $\Delta E_{el} = kx^2/2$, which is compensated by the decrease in the Coulomb energy of electrons, which can be represented as:

$$\Delta W_C = e^2/(4\pi\varepsilon_0\varepsilon r) - e^2/(4\pi\varepsilon_0\varepsilon(r+\Delta x)) = e^2 x/(4\pi\varepsilon_0\varepsilon r) \quad (1)$$

where r-distance between impurity centers, e is the electron charge, ε is the dielectric constant, x = Δx/r is the relative displacement of ions, the bulk density of the Coulomb energy $\Delta E_C = \Delta W_C/V$. From the equality of energies $\Delta E_c = \Delta E_{el}$ we determine the value of the displacement $x = e^2/(4\pi\varepsilon_0\varepsilon r k V)$. For parameters $V = 10^{-27}\ m^3$, $k = 10^{11}\ N/m^2$, r = 1 nm, ε = 50, the relative change in linear dimensions is $x \approx 10^{-3}$. Deformation of the structure, an analogue of pressure, leads to a shift of the chemical potential to the edge of the mobility level (Fig. 8c). At T > 450 K, the conductivity of lattice polarons prevails above the edge of the mobility level.

4. Conclusions

It was shown that substitution of holmium for manganese in the $Ho_XMn_{1-X}S$ with (X = 0.1) causes the instability of the crystal structure of manganese sulfide and the displacement-type structural transition related to the condensation of the polar mode. This transition is accompanied by a change in the paramagnetic Curie temperature, effective magnetic moment, and g factor. The electronic transitions in the $Ho_{0.1}Mn_{0.9}S$ system above room temperature are accompanied by jumps in the temperature dependence of the conductivity and the maxima of the ultrasound attenuation coefficient, the temperatures of which shift in an external electric field. Below room temperature, the sound attenuation is caused by the deformation interaction. The absorption in the far-IR spectral region is related to the splitting of the impurity subbands, as a result of compensation of charged impurities of holmium ions. The high-temperature transition is caused by the pinning of lattice polarons, as a result of which electrons were localized in potential wells induced by holmium ions. The interplay of the electrical, magnetic, and structural characteristics upon temperature variation was established.

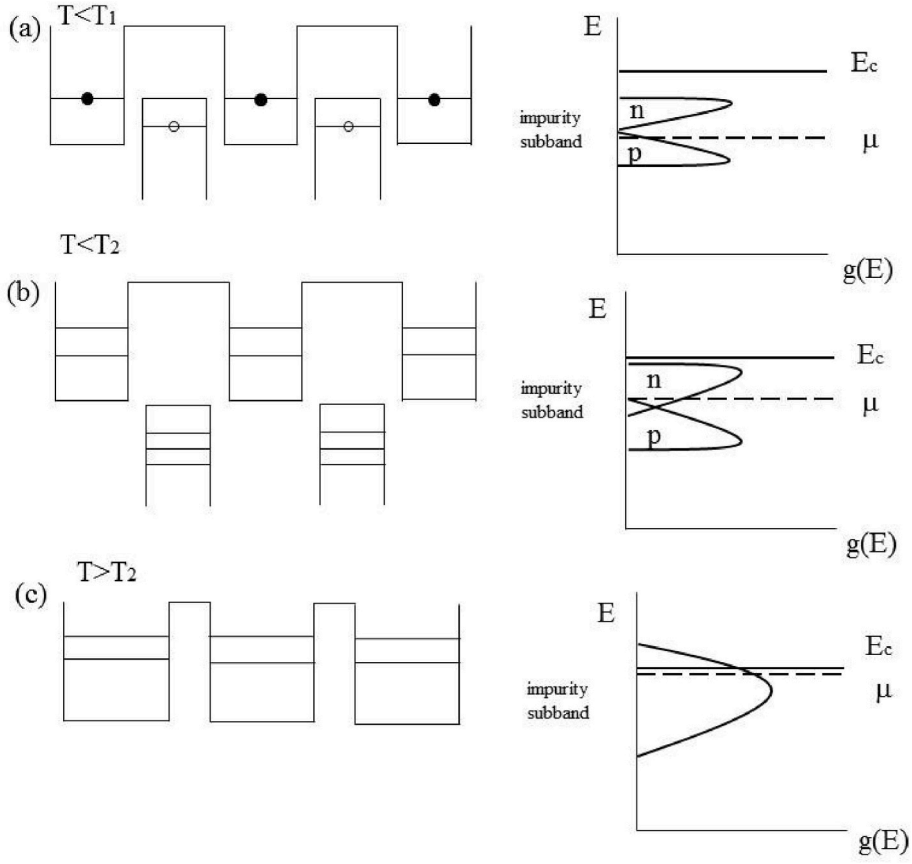

Fig. 8. Potential wells with energy levels filled by holes (empty circles) and electrons (full circles). Electron density state for $Ho_{0.1}Mn_{0.9}S$ below the temperatures phase transitions $T_1 = 340K$ and $T_2 = 450$ K and at temperatures $T > T_2$. Ec – edge of mobility; μ - chemical potential; n-electrons; p-holes.

Author contributions

Romanova O.B: Conceptualization, Investigation, Writing-Reviewing and Editing, **Aplesnin S.S:** Methodology, Writing – original draft. **Sitnikov M.N:** Visualization, Investigation. **Udod L.V:** Supervision, Data curation, **Zelenov F.V:** Investigation.

Declaration of competing interest

The authors declare that they have no known competing financial interests or personal relationships that could have appeared to influence the work reported in this paper.

Data availability

No data was used for the research described in the article.

Acknowledgments

The investigation of microstructural properties of the samples was carried out using equipment's (SEM) the Krasnoyarsk Regional Center of Research Equipment of Federal Research Center « Krasnoyarsk Science Center SB RAS». This work was supported by the Russian Science Foundation, the Government of the Krasnoyarsk Territory, and the Krasnoyarsk Science Foundation project no. 23-22-10016 «The colossal Nernst-Ettingshausen effect in manganese chalcogenides with rare earth substitution».

References

[1] Jun-Ho Kang, Soogil Lee, Taek-Hyeon Lee, Ji-Seok Yang, Jae Wook Lee, Cheong Cheon, Tae, Jong-Ryul Jeong, Seung-Young Park, Byong-Guk Park, Kab-Jin Kim, NPG Asia Mater. 12 (7p) (2020) 44, https://doi.org/10.1038/s41427-020-0222-y.
[2] Y. Guo, J. Dai, J. Zhao, C. Wu, D. Li, L. Zhang, W. Ning, M. Tian, X.C. Zeng, Y. Xie, Phys. Rev. Lett. 113 (5p) (2014), 157202, https://doi.org/10.3938/jkps.61.1545.
[3] L.M. Hrib, L. Pintilie, M. Alexe, Sci. Rep. 7 (9p) (2017) 6563, https://doi.org/10.1038/s41598-017-06487-3.
[4] Xianfeng Liang, Huaihao Chen, Nian X. Sun, Apl. Mater. 9 (2021) 41114–41127, https://doi.org/10.1063/5.0044532.
[5] Tao Wu, Chia-Ming Chang, Tien-Kan Chung, Greg Carman, IEEE Trans. Magn. 45 (2009) 4333–4336, https://doi.org/10.1109/TMAG.2009.2024546.
[6] S.S. Aplesnin, A.M. Kharkov, O.B. Romanova, M.N. Sitnikov, E.V. Eremin, M. V. Gorev, K.I. Yanushkevich, V.V. Sokolov, A.Yu Pichugin, JMMM 352 (2014) 1–5, https://doi.org/10.1016/j.jmmm.2013.09.061.
[7] S.S. Aplesnin, M.N. Sitnikov, O.B. Romanova, A.Yu Pichugin, Phys. Status Solidi B 253 (2016) 1771–1781, https://doi.org/10.1002/pssb.201600134.
[8] O.B. Romanova, S.S. Aplesnin, M.N. Sitnikov, L.V. Udod, J. Exp. Theor. Phys. Lett. 132 (2021) 831–842, https://doi.org/10.1134/S106377612103016X.
[9] O.B. Romanova, L.I. Ryabinkina, V.V. Sokolov, A.Yu Pichugin, D.A. Velikanov, D. A. Balaev, A.I. Galyas, O.F. Demidenko, G.I. Makovetskii, K.I. Yanushkevich, Solid State Commun. 150 (2010) 602–604, https://doi.org/10.1016/j.ssc.2009.12.042.
[10] S.S. Aplesnin, M.N. Sitnikov, A.M. Kharkov, S.O. Konovalov, A.M. Vorotinov, JMMM 513 (2020) 167104–167111, https://doi.org/10.1016/j.jmmm.2020.167104.
[11] S.S. Aplesnin, M.N. Sitnikov, JETP Lett. 100 (2014) 95–101, https://doi.org/10.1134/S0021364014140021.
[12] S.S. Aplesnin, M.N. Sitnikov, O.B. Romanova, A.M. Kharkov, O. Begisheva, F. V. Zelenov, Eur. Phys. J. E 137 (12p) (2022) 226, https://doi.org/10.1140/epjp/s13360-022-02432-0.
[13] S.S. Aplesnin, A.M. Kharkov, M.N. Sitnikov, V.V. Sokolov, JMMM 347 (2013) 10–13, https://doi.org/10.1016/j.jmmm.2013.07.044.
[14] M.N. Sitnikov, S.S. Aplesnin, A.M. Kharkov, O.N. Bandurina, IOP Conf. Ser. Mater. Sci. Eng. 1181 (6p) (2021), 012008, https://doi.org/10.1088/1757-899X/1181/1/012008.
[15] O.B. Romanova, S.S. Aplesnin, M.N. Sitnikov, L.V. Udod, A.M. Kharkov, Appl. Phys. A 128 (9p) (2022) 124, https://doi.org/10.1007/s00339-021-05198-x.
[16] Abdulaziz M. Alanazi, Paul D. McNaughter, Firoz Alam, J. Inigo, Vitorica-yrezabal, George F.S. Whitehead, Floriana Tuna, Paul O'Brien, David Collison, David J.

Lewis, ACS Omega 6 (2021) 27716–277725, https://doi.org/10.1021/acsomega.1c02907.
[17] J.K. Clark, V. Yannello, A.M. Samarakoon, C. Ross, M.C. Uible, V.O. Garlea, M. Shatruk, J. Phys. Chem. C 125 (2021) 16183–16190, https://doi.org/10.1021/acs.jpcc.1c02956.
[18] B. Morosin, Phys. Rev. B 1 (1970) 236–243, https://doi.org/10.1103/PhysRevB.1.236.
[19] S.S. Aplesnin, L.I. Ryabinkina, G.M. Abramova, O.B. Romanova, A.M. Vorotynov, D.A. Velikanov, N.I. Kiselev, A.D. Balaev, Phys. Rev. B 71 (2005) 125204–125208, https://doi.org/10.1103/PhysRevB.71.125204.
[20] H.H. Heikens, G.A. Wiegers, C.F. van Bruggen, Solid State Commun. 24 (1977) 205–209, https://doi.org/10.1016/0038-1098(77)91198-X.
[21] L. Bragg, G.F. Claringbull, Crystal Structures of Minerals, MIR, Moscow, 1967.
[22] V.S. Urusov, Theory of Isomorphic Miscibility, Nauka, Moscow, 1977.
[23] K.S. Aleksandrov, A.T. Anistratov, B.V. Beznosikov, N.V. Fedoseeva, Phase Transitions in Crystals of the Halide Compounds ABX_3, Nauka, Novosibirsk, 1981.
[24] A. Amorese, B. Leedahl, M. Sundermann, H. Gretarsson, Z. Hu, H.-J. Lin, C.T. Chen, M. Schmidt, H. Borrmann, Yu Grin, A. Severing, M.W. Haverkort, L.H. Tjeng, Phys. Rev. X 11 (2021) 11002–11011, https://doi.org/10.1103/PhysRevX.11.011002.
[25] G. Nolze, C. Grosse, A. Winkelmann, J. Appl. Crystallogr. 48 (2015) 1405–1419, https://doi.org/10.1107/S1600576715014016.
[26] S.A. Mousavi, A. Hekmarti, M. Sedighizaden, M. Begdeli, A. Bazargan, TSEP 20 (2020) 100671, https://doi.org/10.1016/j.tsep.2020.100671, 15.
[27] O. Bidaut, P. Goux, M. Kchikech, M. Belkaoumi, M. Magione, Phys. Rev. B 49 (1994) 7868–7873, https://doi.org/10.1103/PhysRevB.49.7868.
[28] J.P. Hague, P.E. Kornilovitch, A.S. Alexandrov, Phys. Rev. B 78 (2008), 092302, https://doi.org/10.1103/PhysRevB.78.092302. – 4.
[29] G. Geneste, B. Amadon, M. Torrent, G. Dezanneau, Phys. Rev. B 96 (2017) 134123, https://doi.org/10.1103/PhysRevB.96.134123, 13.
[30] S.S. Aplesnin, Magnetic and Electrical Properties of Strongly Correlated Magnetic Semiconductors with Four-Spin Interaction and with Orbital Ordering, Fizmatlit, Moscow, 2013.
[31] W. Cochran, A. Zia, Phys. Status Solidi 25 (1968) 273–283, https://doi.org/10.1002/pssb.19680250126.
[32] L.V. Udod, S.S. Aplesnin, M.N. Sitnikov, O.B. Romanova, M.N. Molokeev, J. Alloys Compd. 804 (2019) 281–287, https://doi.org/10.1016/j.jallcom.2019.07.020.
[33] H. van der Heide, C.F. van Bruggen, G.A. Wiegers, C. Haas, J. Phys. C Solid State Phys. 16 (1983) 855–868, https://doi.org/10.1088/0022-3719/16/5/012.
[34] J. Van den Brink, D.I. Khomskii, Multiferroicity due to charge ordering, J. Phys. Condens. Matter 20 (12p) (2008), 434217, https://doi.org/10.1088/0953-8984/20/43/434217.
[35] F. Battista, A. Camjayi, L. Arrachea, Phys. Rew. B 96 (2017), 045413, https://doi.org/10.1103/PhysRevB.96.045413. – 7.